AN AVALANCHE TRANSISTOR COINCIDENCE CIRCUIT
FOR USE WITH THE ORANGE SPECTROMETER

by

John C. Hardy

A thesis submitted to the Faculty of Graduate Studies and Research of McGill University in partial fulfillment of the requirements for the degree of Master of Science.

July 1963

Radiation Laboratory
McGill University
Montreal

TABLE OF CONTENTS

LIST OF FIGURES AND TABLES

ACKNOWLEDGEMENTS

Virtually all members of the Radiation Laboratory have assisted me in one way or another during the preparation of this thesis. In particular I wish to thank: Professor R.E. Bell, my research director, for his advice; Mr. G.X. Amey who suggested the use of avalanche transistors to me, and whom I consulted frequently in their application; and especially Mr. G.R. DeMille who very generously helped me, both mentally and physically, with all parts of the work relating to the spectrometer.

I am also grateful to Dr. J. Crawford who, in Dr. Bell's absence, checked the manuscript.

1. INTRODUCTION and SUMMARY

This thesis describes the use of avalanche transistors in a circuit for measuring delayed coincidences. Using the circuit, the time characteristics of the β-ray Orange Spectrometer are determined to be such that for most coincidence measurements the lower limit of resolution will be determined primarily by the photomultipliers and scintillators, and not the spectrometer. A method for calculating the electron path lengths - and so, times of flight - which can be applied to spectrometers of this type is outlined and tested.

The circuit provides a ready means for measuring the time characteristics of the avalanche transistor itself, and such a study is made. On this basis it is shown that the coincidence only "sees" the photomultiplier pulse for that instant at which it reaches a certain predetermined voltage. An analysis by Gatti and Svelto (1959) indicates that this method of extracting time information should give somewhat poorer time resolution than conventional methods which average over some part of the photomultiplier pulse (see also M.A. El-Wahab and J.V. Kane, 1962). This seems to be borne out by the fact that the minimum resolution which was found with this circuit of 3×10^{-10} seconds is slightly worse than that obtained at this laboratory with a more conventional circuit, although comparison is difficult since different photomultipliers and scintillators were used. An investigation is made of the dependence of resolution on the point on the photomultiplier pulse at which the avalanches trigger, and the results are compared to the predictions of Gatti and Svelto; the agreement is good.

Finally, to demonstrate the operation of the system, the mean lives of positrons in aluminum are measured and found to be essentially in agreement with the results of Bell and Jørgensen (1960).

2. AVALANCHE CIRCUITRY

2.1 Avalanche Breakdown

Suppose a reverse voltage is applied to a p-n junction. As this voltage is increased from zero, a small current will flow; for moderate voltages, it will be constant ($= I_{CO}$) - its value determined by the density of minority carriers. If the voltage is increased farther, however, the minority carriers which are accelerated in the high field region of the junction begin to have enough energy to produce hole-electron pairs by collision. Thus, a multiplication process is initiated. This multiplication increases with applied voltage and becomes essentially infinite at the "breakdown voltage", V_B. Empirically:

$$M = \frac{1}{1 - (V/V_B)^n} \qquad (1 - A)$$

where "n" depends on the semiconductor, but is typically around 4.

2.2 Avalanche Transistor

The usefulness of this process was first indicated by Miller and Ebers (1955). They pointed out that for a transistor there would be, in effect, two breakdown voltages. Between the base and collector (emitter open) this voltage would be the previously described V_B; while between emitter and collector (base open) it would be a smaller value, V_S. V_S can be shown to be the voltage at which the total current gain, α, equals one. (If α_o is the current gain at low voltage, then $\alpha = \alpha_o M$.) The relationship between V_S and V_B follows directly from (1 - A):

$$V_S = V_B (1 - \alpha_o)^{1/n} \qquad (1 - B)$$

Consider the circuit in figure 1a; it is equally valid for npn and pnp transistors although it is only drawn for the pnp type. Normally the base is held at a reverse bias with respect to the emitter, and consequently the impedance of the emitter-base junction will be high. For this reason, most of the current will flow through the base circuit - providing, of course, that its external resistance, R_B, is relatively small - and, for V_T large, the voltage at point "A" will be very nearly equal to V_B. Now, if the emitter-base impedance can be reduced - say by applying a pulse of the appropriate sign to the base - the current will switch from the base to the emitter circuit. This has the effect of decreasing the voltage at point "A" towards V_S, and discharging capacitor C. A pulse will be produced across R_L. As the available current decreases, the base-emitter impedance again increases and the capacitor begins recharging to V_B. When the voltage reaches V_B, the cycle may be repeated.

The specific properties of this process depend strongly on the transistor used, and a number of transistors have been investigated in this context. (See, for example, R. Fullwood, 1960; W.M. Henebry, 1961; H.W. Miller and Q.A. Kerns, 1962.) In general, transistors most suited to the process will have large α_o and small n; the reasons for this are readily apparent from equation (1 - B). For a suitable choice, avalanche voltages (across resistor R_L) as high as 100 volts may be obtained. Of the transistors reported upon, most exhibited an avalanche pulse risetime of the order of a nanosecond and could be triggered by less than half a volt. Fast switching germanium pnp types seemed the most favourable.

The basic circuit has been modified in a number of ways, usually for the purpose of generating pulses of short duration and fast rise- and fall-time (Fullwood, 1960; Henebry, 1961; Miller and Kerns, 1962; M. Bramson, 1962.) with, in one case, (Bramson) a repetition rate as high as 10 megacycles.

2.3 Circuit Used

a) Requirements: A circuit was desired which could be activated by a negative pulse from the plate of a photomultiplier tube to produce a pulse of very short risetime which remained greater than 2 volts for at least 60 nanoseconds - the latter condition being in order to meet the requirements of the time to amplitude converter.

b) Transistor: The transistor which seemed the most suitable at the time was the ASZ23. It is a pnp post alloy diffused germanium junction transistor which will give a 15 volt pulse across 200 ohms with a risetime of 1 nanosecond. It is by no means the only possible choice.

c) Circuit Elements: The restriction upon R_C is that it be large enough to keep the quiescent current in the collector-base circuit low enough to prevent "latching up" (Bramson, 1962) and overheating the transistor. The manufacturer suggests 1 ma.

The choice of R_B is quite critical: As explained in 2.2, it must be small compared to the base-emitter impedance; but it cannot be too small. This point is demonstrated by figure 2. The voltage-current characteristics of the circuit configuration shown in part (a) of that figure are found by using a Tektronix Type 575 Transistor-Curve Tracer. There are three distinct regions to these curves: At low currents, the resistance is very high; then, after breakdown, there is a region of negative resistance; finally, for higher current, the resistance is practically zero. For best performance, it is evident that the second region should be as small as possible. The curves in figure 2b show the effect of different values of R_B; for R_B greater than 1K, there was little change in the last two regions while the size of the maximum voltage continued to decrease. In the light of these considerations, $R_B = 1K$ was determined upon.

The pulse length desired (2.3 a), dictated that C be, at least, 500pf.

The final values chosen are shown in figure 4 while the resulting pulse shapes at several points appear in figure 1b.

d) Biasing: The maximum allowable reverse emitter-base voltage for the ASZ23 is 2 volts. Thus, by making the bias variable, it should be possible to discriminate over that range. In fact, Fullwood (1960) has shown that the 2N504 under similar conditions has quite sharp discriminating characteristics; however, he made no investigation of the time jitter as a function of the discriminator setting.

e) False Triggering: It is an unfortunate property of the high sensitivity of the avalanche circuit that triggering can take place almost as readily at the collector or emitter as it can at the base - although, for the emitter, a positive trigger is required. Consequently to prevent "false triggering", care must be taken in the matching of cables and in the isolation of one avalanche circuit from the other. Precautions taken in this regard will be dealt with in the following section.

FIGURE 1 :

(a) Basic Avalanche circuit. See section 2.2 .

(b) Pulse shapes at two points for circuit components as in figure 4; ie R_B = 1K, R_C = 180K, C = 500pf, R_L = 185Ω. See section 2.3 .

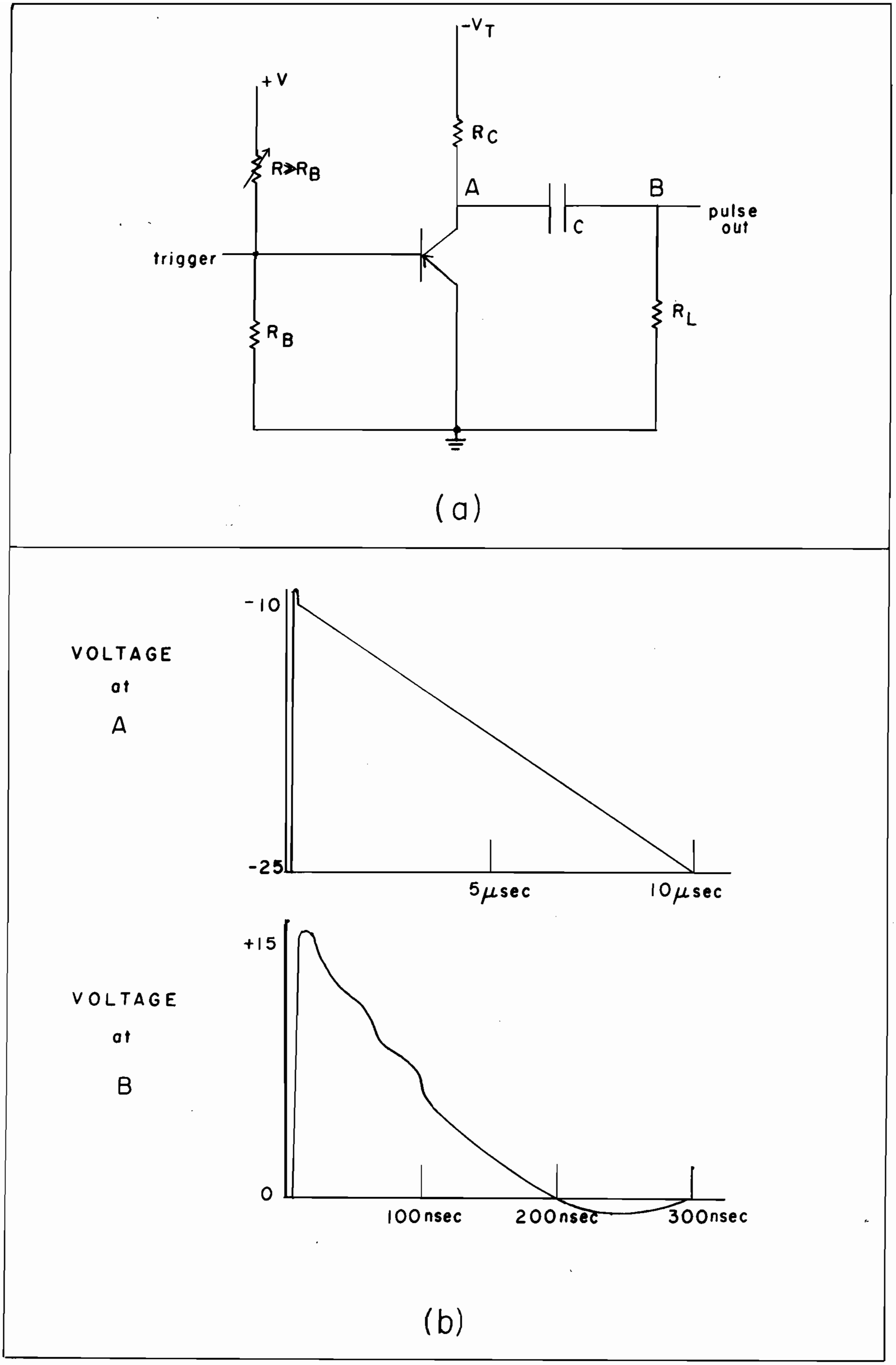
-V_T
+V
R_C
R>R_B
A
B
C
pulse out
trigger
R_B
R_L
(a)
-10
VOLTAGE at A
-25
5μsec
10μsec
+15
VOLTAGE at B
0
100nsec
200nsec
300nsec
(b)

FIGURE 1

<u>FIGURE 2</u> :

(a) Circuit configuration tested.

(b) Facsimile of the Curve Tracer display for the ASZ23 transistor and several values of R_B. See section 2.3 .

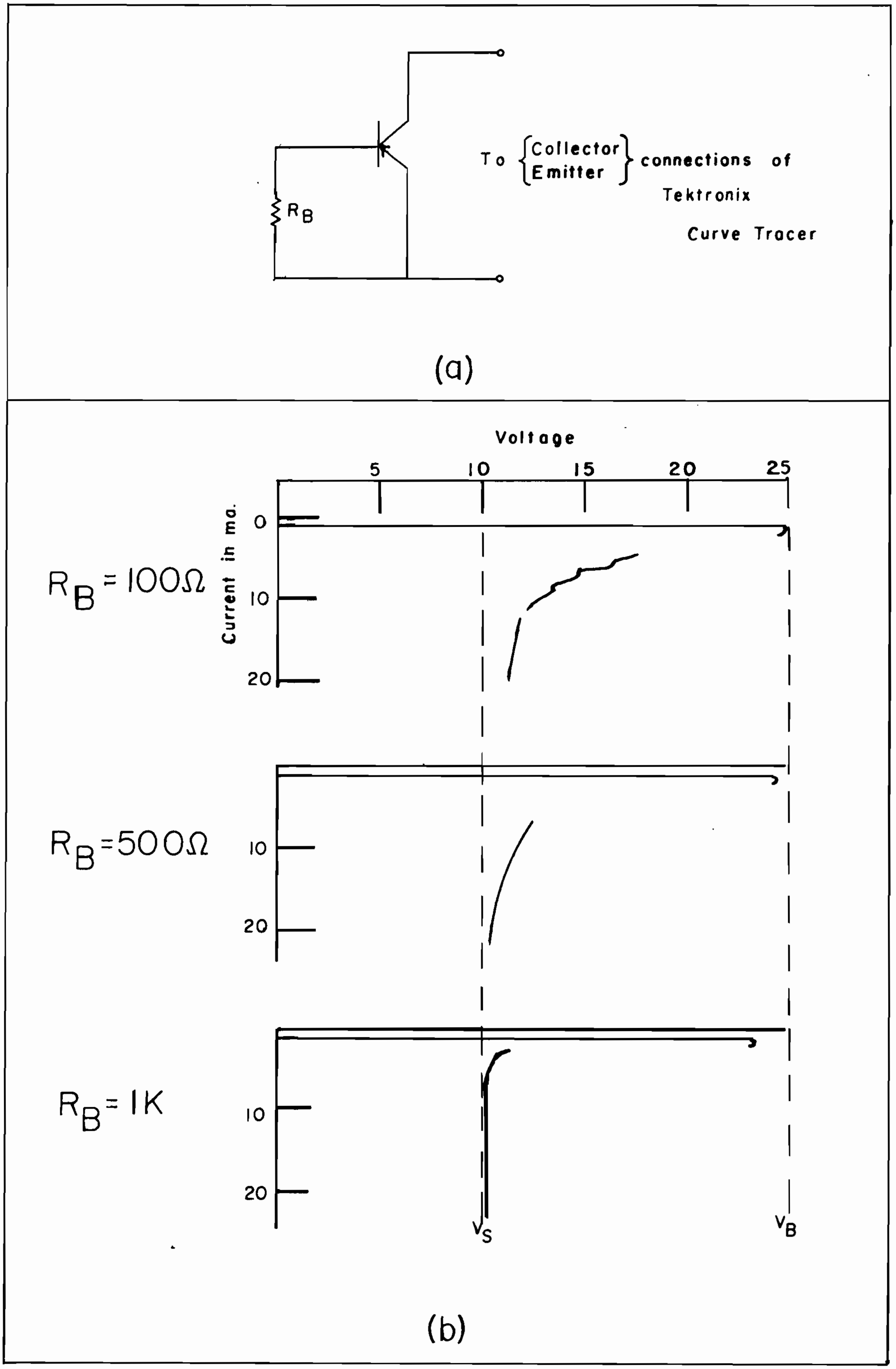

R_B
To {Collector / Emitter} connections of Tektronix Curve Tracer
(a)
Voltage
5
10
15
20
25
Current in ma.
0
10
20
$R_B = 100\Omega$
$R_B = 500\Omega$
$R_B = 1K$
V_S
V_B
(b)

FIGURE 2.

3. EXPERIMENTAL APPARATUS

3.1 Outline

A block diagram of the apparatus used is shown in figure 3, where it is divided into three main sections: time; energy; and reference circuits.

The first two comprise what is generally referred to as a fast-slow coincidence circuit; it is similar in concept to the one described by Bell et al (1952): For example, if a signal from photomultiplier 2 appears, in this case, within 30 nanoseconds after a signal from photomultiplier 1, then the time (or fast) circuit produces a time-analogue pulse whose height corresponds to their time-separation. Simultaneously, the energy (or slow) circuit energy-selects the signals according to predetermined specifications and produces gate pulses if the conditions are met. The presence of two gate pulses permits the corresponding time-analogue pulse to be registered in the multichannel analyzer. Thus, although the separation of all such pairs of pulses is measured, only those measurements representing a chosen pair of energy transitions are actually recorded.

3.2 Time ("Fast") Circuit

The components of the time circuit are shown in detail in figures 4 and 5.

a) Standard Pulse Formation: Negative pulses from the anode of each photomultiplier are fed through an emitter follower onto the base of an avalanche transistor connected in the manner already described. Those pulses above the discriminator level will fire the transistor, giving rise to a signal of standard shape and size.

b) Limiting, Clipping, and Adding: A pair of simple current switches with a common output resistor are used to limit and add the pulses from the two avalanche circuits, while a 30 nanosecond length of shorted RG-62/U, 93 ohm cable connected across the output serves to clip the pulses to 60 nanoseconds in length. The lengths of the cables leading from the avalanche circuits to the limiters are such that two events which are simultaneous at the photomultipliers will produce pulses at the output of the current switches whose leading edges are separated by 30 nanoseconds. To prevent any reflections from reaching the time to amplitude converter, these cables were matched at both ends; they were series matched at the avalanche end since reflections would always appear at that point while the transistor was still conducting across the low resistance base-emitter junction.

An advantage of the present system is that 93 ohm cable can be used for the clipping cable as well as for the "delay" cables since the former can be matched independently of the latter. This removes the necessity for using cables of different impedance and eliminates the concomitant loss in pulse height inherent in most previous systems.

Although the diodes in the current switch provide a relatively high degree of isolation of one avalanche circuit from the other, it was found that under some bias conditions false triggering did occur. (See 2.3 e) Since a pulse reaching the clipping line is not initially rectangular, the positive clipped pulse will be followed by an irregular negative one; the small fraction of this negative pulse which reaches the collector of the unfired avalanche transistor may, in some cases, be enough to fire it. However, since the first transistor cannot be refired immediately*, it is evident that such an occurence could never result in a false coincidence.

c) Time to Amplitude Converter: The time to amplitude converter is identical to one used previously in this laboratory (R.S. Weaver, 1962). It is made up of another two-diode current switch which is biased so that current will be switched to the integrating capacitor only if the sum of two pulses appears at the input. The capacitor charges for the length of time which the input pulse spends above the set level.

This provides a highly linear time-analogue pulse which is then shaped and amplified.

3.3 Energy ("Slow") Circuit

Energy-selection was performed on the positive pulses from the last (tenth) dynode of the photomultiplier tubes; only conventional circuit elements were used. (See figure 3.)

3.4 Reference Circuit

The reference circuit serves a dual purpose: it may be used to calibrate the system; and to produce a reference "coincidence", say

---

* The dead-time of the circuit is determined by the length of time required to recharge capacitor C (fig. 1) and is long compared to the length of the avalanche pulse.

once a second, during a counting period in order to monitor possible drifts or malfunctions of the system. Although it does not correct drift in any way, this latter function does provide a means whereby accurate centroid shift measurements can be made, even if moderate drifts have occurred, simply by measuring centroids relative to that of the reference "peak".

Reference Pulser: The so-called reference pulser is shown in figure 6; it is simply an avalanche circuit which produces equal positive and negative pulses, continuously variable from zero to three volts, and with a risetime of the order of a nanosecond. It is triggered by less than one volt negative, but is unharmed by large pulses of either sign. In fact, it is successfully triggered from the register output of a Scale of 64 (Atomic Instrument Company, Model 101-M) which is a 20 volt pulse and positive.

The negative output from the pulser was fed into a junction point on a 10 meter long air-cored delay line, and thence to the emitter followers at the plate of each photomultiplier tube. This method has been described previously by Graham et al (1962).

It was desirable that the reference pulse should give rise to a time-analogue pulse of essentially the same height as that of a true prompt coincidence. However, any counting-rate dependence in the system results in a tail to the reference peak which, at best, increases the apparent chance rate. For this reason, it was decided to divide the Victoreen 400 channel analyser into two 200 channel units. The first unit, which would normally record the energy-selected time pulses, would be gated off for 5 microseconds during and after the appearance of a reference pulse; for the same time, the second unit would be gated on. Thus, the spectrum stored in unit one will be the usual delayed (or prompt) coincidence curve.

Unit two will display all counts associated with the reference coincidences. From this, two things may be learned: the extent of the drift during the counting period; and the effect on the system of the counting rates used. This latter point will be discussed in some detail later.

FIGURE 3 :

Block diagram of the apparatus used. See section 3.1 .

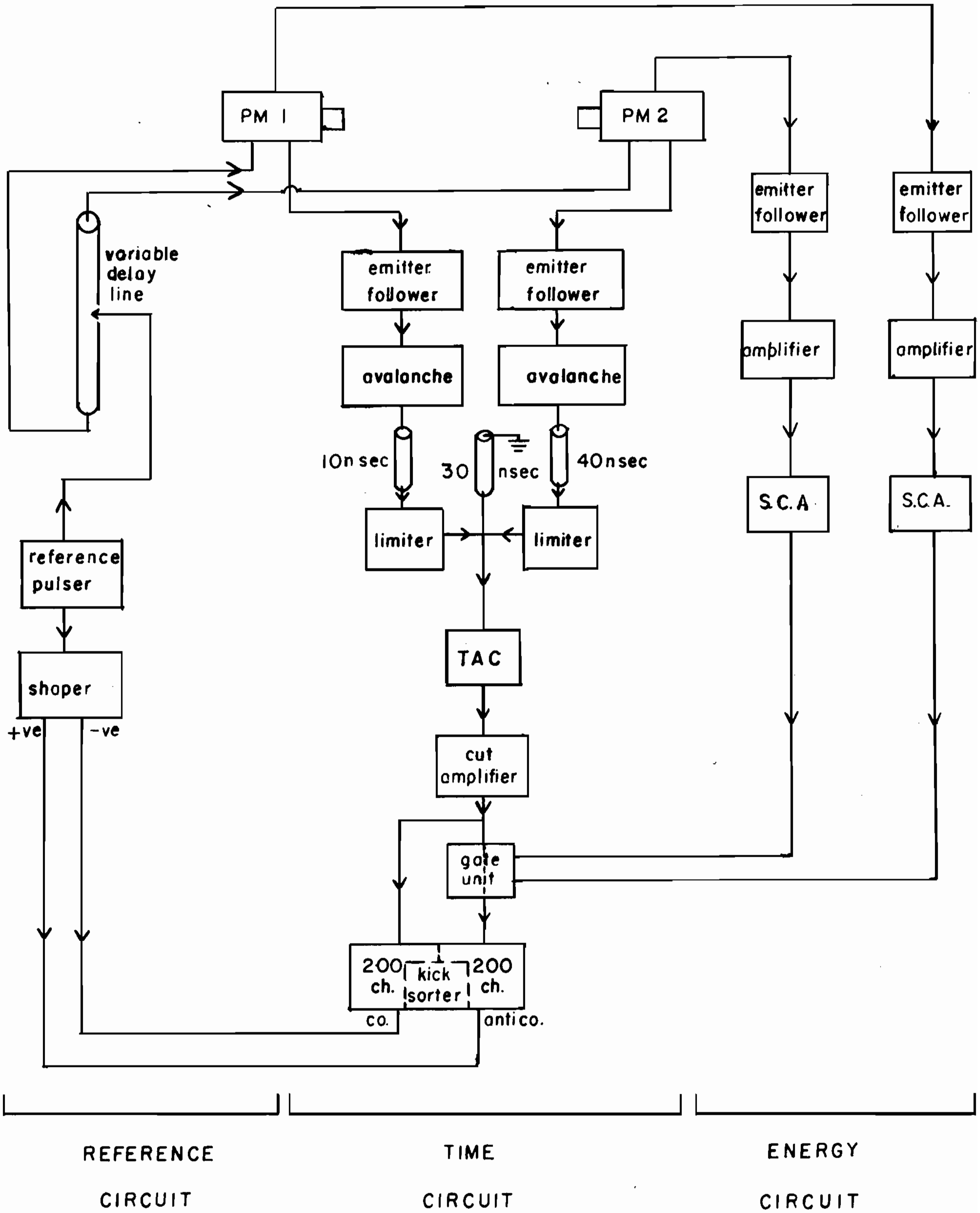
PM 1
PM 2
variable delay line
emitter follower
emitter follower
emitter follower
emitter follower
avalanche
avalanche
amplifier
amplifier
10n sec
30 nsec
40nsec
S.C.A
S.C.A.
limiter
limiter
reference pulser
shaper
+ve
-ve
TAC
cut amplifier
gate unit
200 ch.
kick sorter
200 ch.
co.
antico.
REFERENCE CIRCUIT
TIME CIRCUIT
ENERGY CIRCUIT

FIGURE 3

FIGURE 4 :

Diagram of the photomultiplier, emitter follower, and avalanche circuits. See section 3.2 .

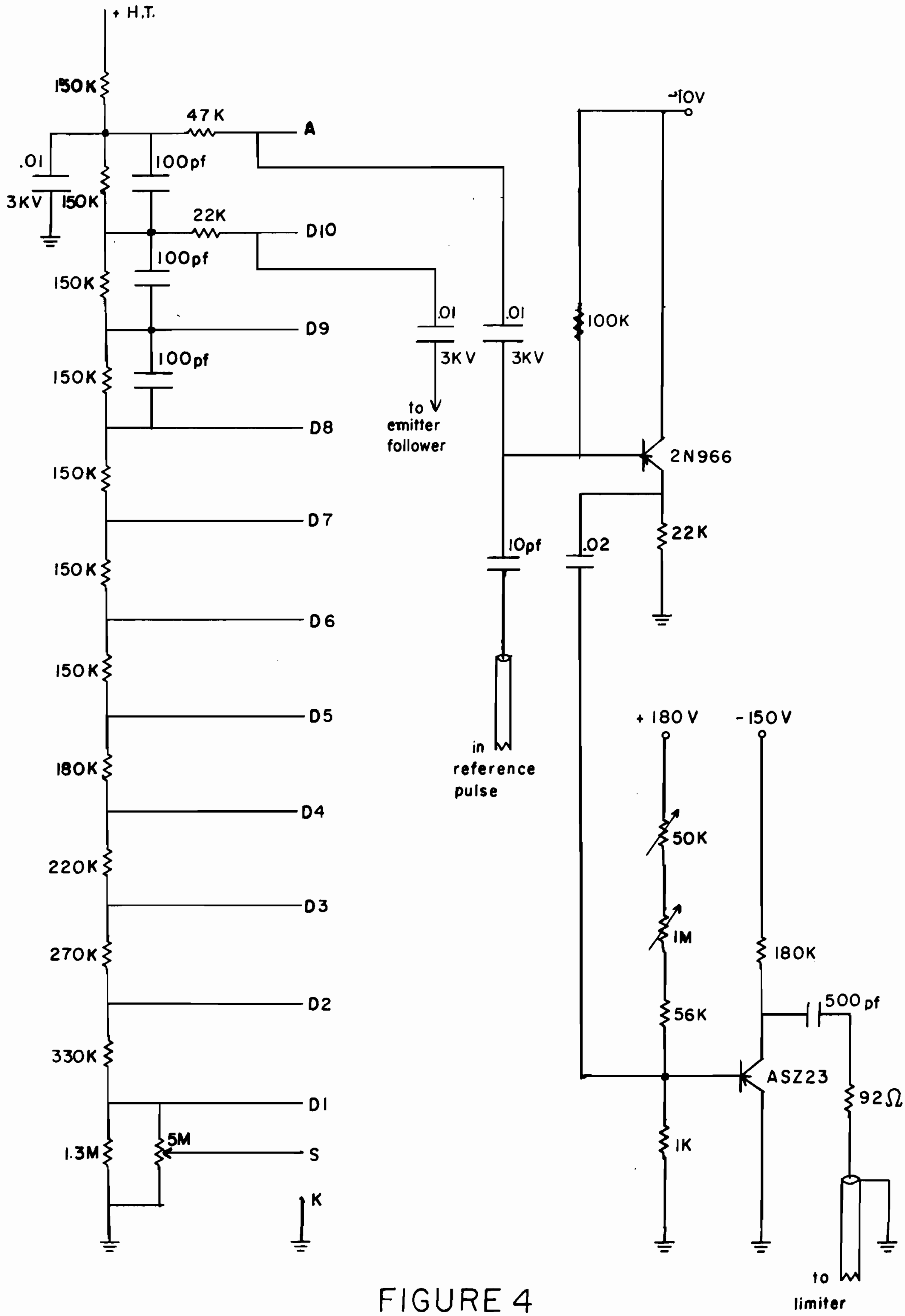
+ H.T.
150K
47K
A
.01
3KV
150K
100pf
22K
D10
100pf
150K
D9
100pf
150K
D8
150K
D7
150K
D6
150K
D5
180K
D4
220K
D3
270K
D2
330K
D1
1.3M
5M
S
K
.01
3KV
to
emitter
follower
.01
3KV
10pf
in
reference
pulse
-10V
100K
2N966
22K
.02
+ 180 V
- 150 V
50K
1M
56K
1K
180K
500 pf
ASZ23
92Ω
to
limiter

FIGURE 4

FIGURE 5 :

Diagram of the limiters, time to amplitude converter, and amplifier circuits. See section 3.2 .

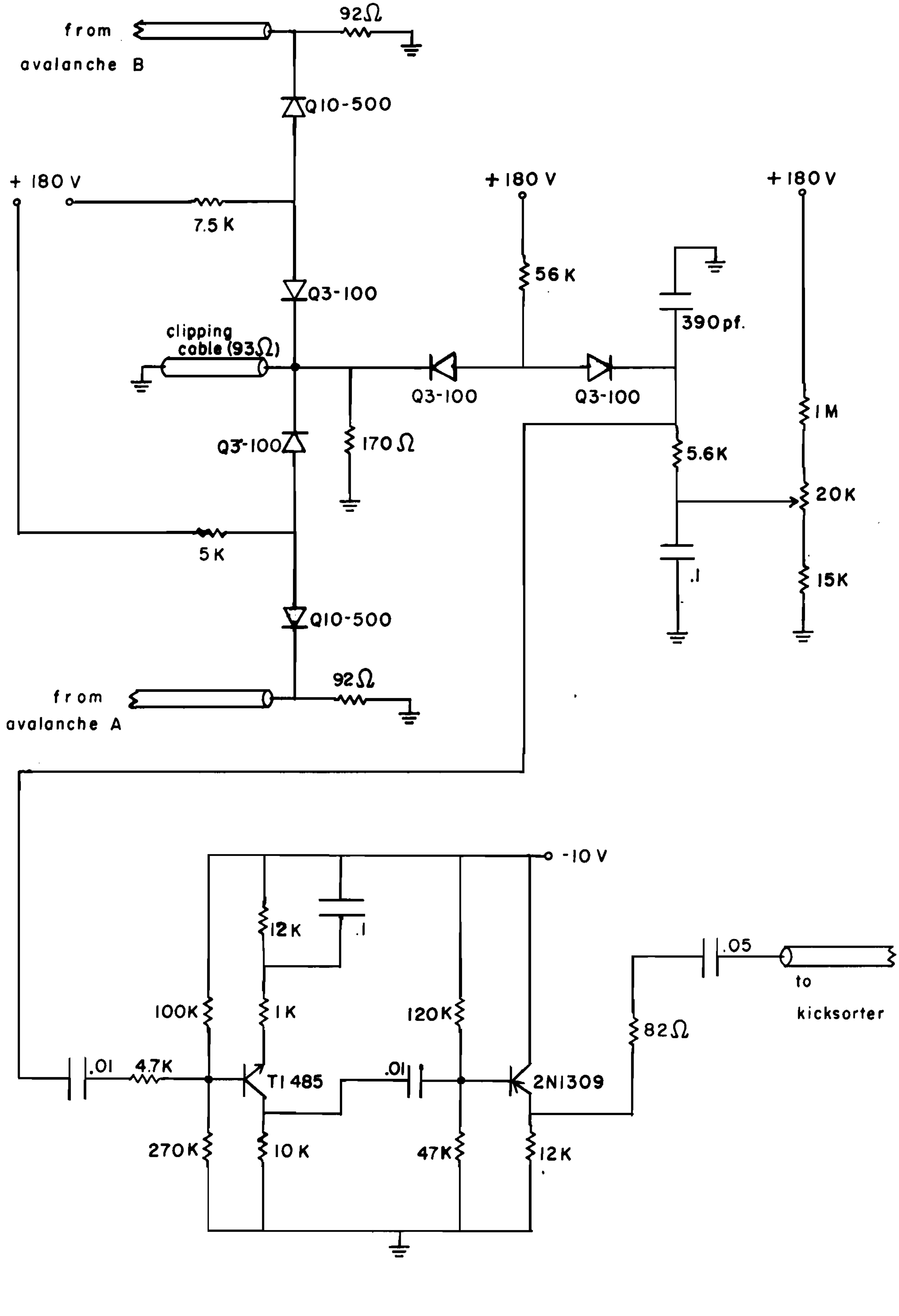
from
avalanche B
92Ω
Q10-500
+ 180 V
7.5 K
Q3-100
clipping
cable (93Ω)
Q3-100
170 Ω
5 K
Q10-500
from
avalanche A
92Ω
+ 180 V
56 K
Q3-100
Q3-100
390 pf.
5.6K
.1
+ 180 V
1 M
20K
15K
-10 V
12 K
.1
100K
1 K
120K
.01
4.7K
TI 485
.01
2N1309
270K
10 K
47K
12K
82Ω
.05
to
kicksorter

FIGURE 5.

FIGURE 6 :

Circuit diagram of the reference (avalanche) pulser. See section 3.4 .

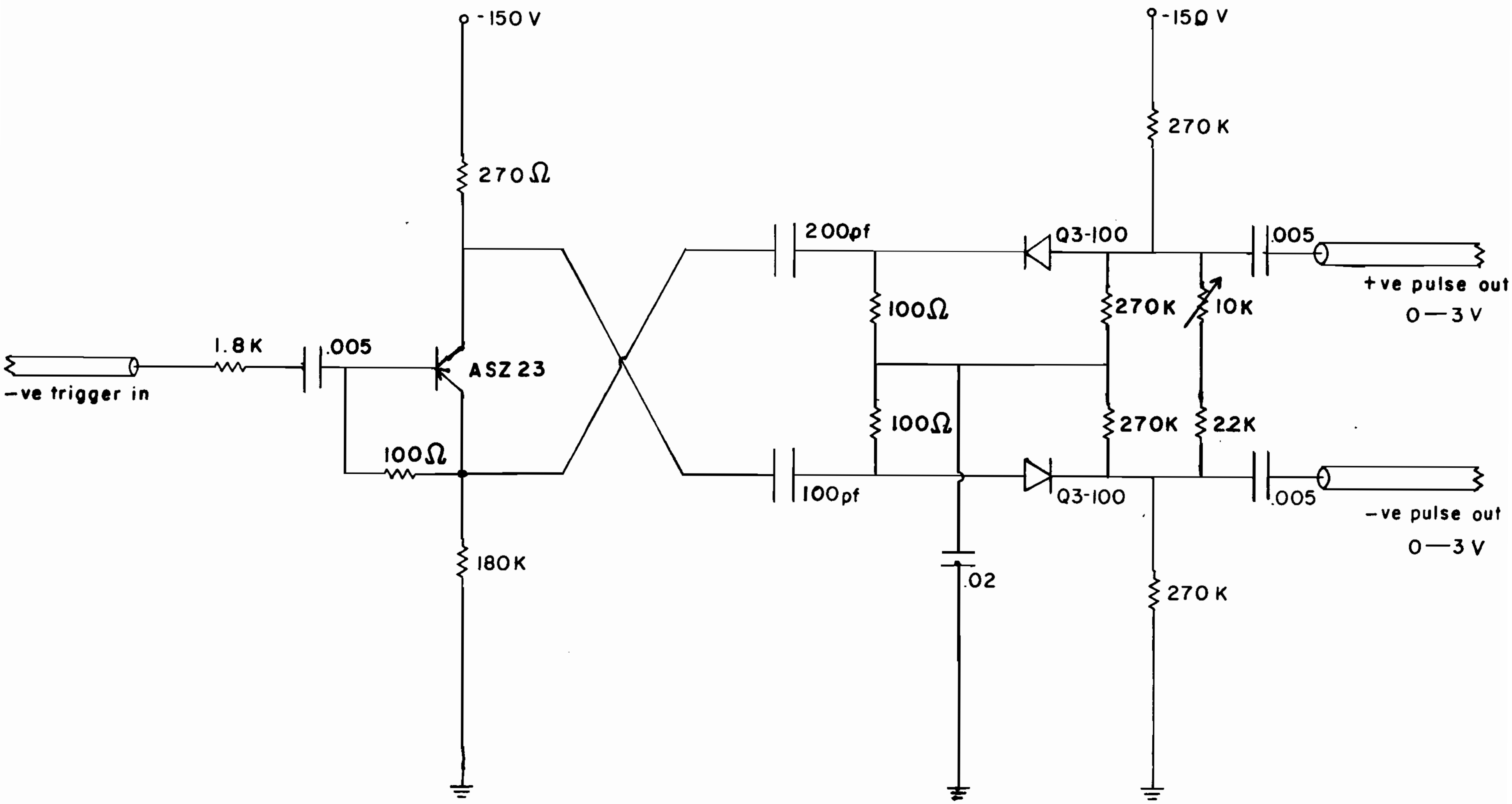
-150 V
270Ω
-ve trigger in
1.8 K
.005
ASZ 23
100Ω
180 K
200pf
100pf
100Ω
100Ω
.02
Q3-100
Q3-100
-150 V
270 K
270K
270K
10K
2.2K
270 K
.005
.005
+ve pulse out
0—3 V
-ve pulse out
0—3 V

FIGURE 6

4. THE β-RAY (ORANGE) SPECTROMETER

4.1 General

In 1950, a new kind of β-ray spectrometer was proposed by Kofoed-Hansen, Lindhard, and Nielsen. It offered the advantage of having a very large transmission as well as good energy resolution. Also, the source and focus were both in regions of zero magnetic field, which would allow photomultiplier tubes to be brought near both points. The instrument was to consist of six wedge-shaped pole pieces separated by air gaps of the same shape, and placed, like the segments of an orange, symmetrically around the axis which passes through source and focus. Such a spectrometer was subsequently built and successfully tested (O.B. Nielsen and O. Kofoed-Hansen, 1955).

A spectrometer based on the same principle but made up of only a single gap has been constructed at this laboratory by G.R. DeMille; he has measured the transmission and momentum resolution of this instrument to be 1% and 2% respectively (See References: G.R. DeMille.). These values are similar to the corresponding ones for our Slatis-Siegbahn spectrometer which was built earlier (J. Hilborn, 1954). However, if it was to be considered for very short β-γ lifetime measurements, its time resolution also had to be measured.

4.2 Transmission, and Time Resolution

A vertical cross-section taken parallel to the axis of the spectrometer is shown in figure 7. The diaphragm between the source and pole pieces served to divide the aperture into a series of ten regions which could be investigated separately. To conform with earlier literature (Nielsen and Kofoed-Hansen, 1955), these will be referred to as diaphragms 1 through 10. Clearly, the transmission through each will not be the same; not only will there be the dependence on sin θ, but imperfections due to the fringing field will seriously affect the transmission of electrons whose paths are near the boundaries of the pole pieces. The effect may be seen in table I, where the transmissions for diaphragms 1, 2, 3, and 10 are seen to be very small. The measurements were made by G.R. DeMille using the K-conversion electrons from the 661 KeV transition in Cs^{137}.

Estimates of the path lengths involved indicated that the time of flight of an electron passing through diaphragm 10 would be at least a nanosecond greater than that of one through diaphragm 2. The time spread with any one diaphragm might then be expected to be of the order of 10^{-10} seconds. Consequently, it should be possible, by combining several diaphragms, to have both a fairly high transmission and a time resolution of less than half a nanosecond.

More precise calculations and relevant measurements were made and will be discussed in the following sections.

TABLE I

Properties of each Diaphragm

for the Orange Spectrometer:

Diaphragm number:	Angle of emission, θ:	Spread in angle, $\delta\theta$:	Measured Transmission (total = 1%):
1	141°	5°	.00
2	136°	5°	.03
3	131°	6°	.04
4	124°	7°	.10
5	116°	8°	.10
6	108°	9°	.08
7	98°	11°	.16
8	87°	11°	.24
9	77°	10°	.20
10	68°	9°	.06

(all values $\pm$ .02)

<u>FIGURE 7</u> :

A vertical cross-section of the Orange Spectrometer, taken parallel to its source-focus axis. See section 4.2 .

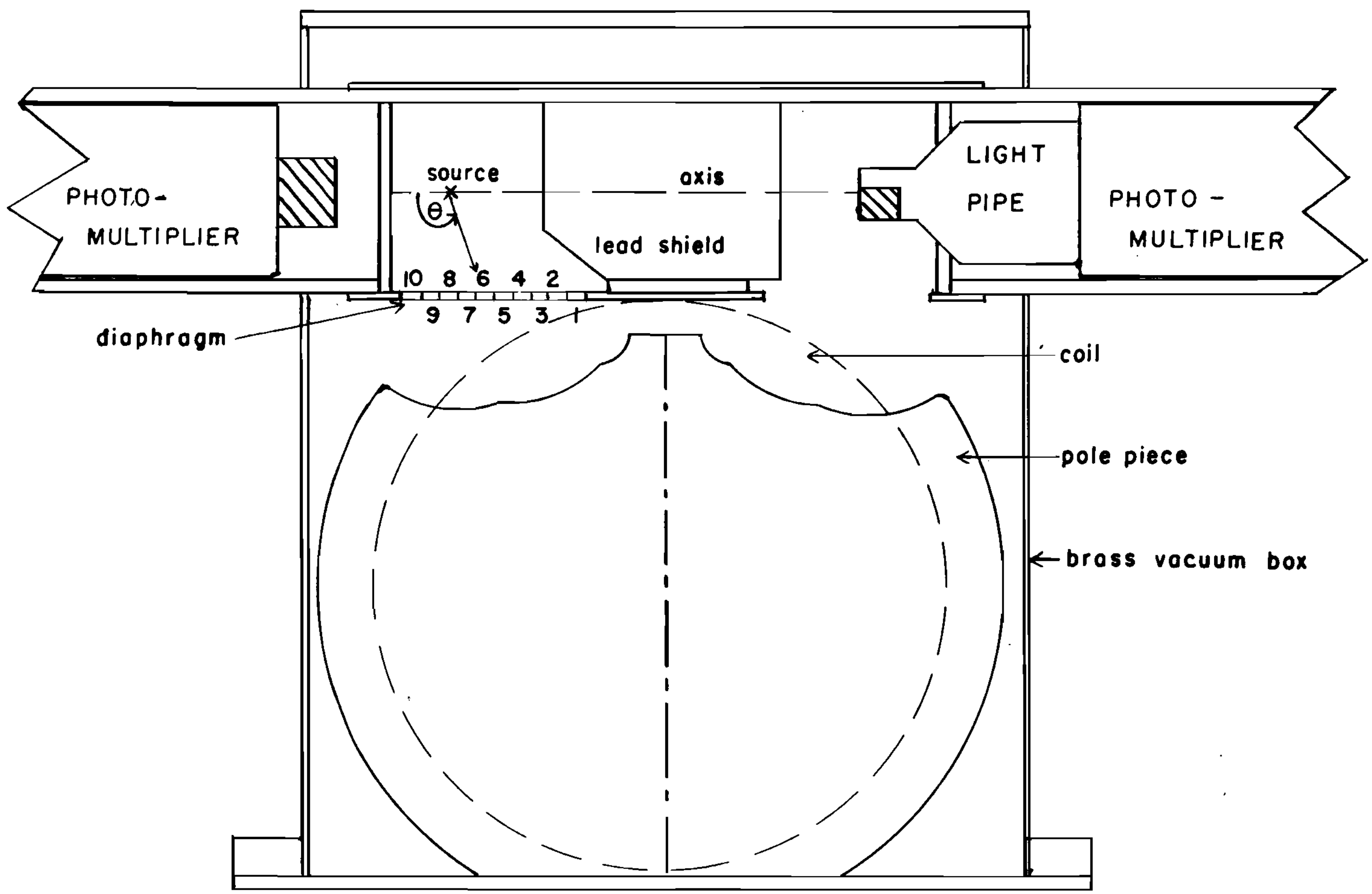
PHOTO-
MULTIPLIER
source
θ
axis
lead shield
LIGHT
PIPE
PHOTO -
MULTIPLIER
10 8 6 4 2
9 7 5 3 1
diaphragm
coil
pole piece
brass vacuum box

FIGURE 7

5. CIRCUIT PROPERTIES

PART I: TRIGGERING

5.1 Introduction

Since the avalanche transistor is potentially so valuable for many applications, it is of interest to investigate its properties as thoroughly as possible. Much work of this kind has already been done by the authors referred to in section 2; it appears, however, that no precise measurements have been made of the dependence of the propagation delay on the size and shape of the trigger pulse. (The "propagation delay" may be defined as the time delay between the instant of triggering and the start of the avalanche pulse.) For fast coincidence work this is of the utmost importance, and so propagation delay measurements were attempted.

5.2 Measurement Technique

The avalanches were connected as in the time circuit of figure 3. One was triggered by a pulse of fixed amplitude, well above the discriminator level, while the other was triggered simultaneously by a pulse whose amplitude and length could be varied. The time analogue pulses were recorded by the kicksorter. In these measurements the trigger pulses were generated by an E.H. Model 120D Pulse Generator, and had a risetime of 1 nanosecond and a duration which was variable from 10 to 100 nanoseconds; their amplitude was varied by clipping with a biased diode, in order to ensure that the voltage rate of increase of the leading edge remained unchanged. These pulses did not have perfectly flat tops, and ultimately it is their unevenness which determines the accuracy of the measurements.

For a given trigger amplitude, the kicksorter time spectrum yielded the following information: the number of times the avalanche had fired was found from the total number of counts recorded in the test period; the time jitter in the propagation delay appeared as the width of the peak; and the relative length of the delay could be determined from the position of the centroid of the peak. The absolute value of the delay was determined (to lower accuracy) by using a Tektronix Type 661 Sampling Oscilloscope.

5.3 Results

A typical set of results is shown in figure 8; similar ones were obtained at other bias settings. It can be seen that for triggers more than 0.3 volts above the discriminator, the propagation delay is constant. The sampling oscilloscope showed that the separation between the leading edges of such a trigger and avalanche pulse was approximately 3 nanoseconds. This result was then compared to that obtained with a trigger pulse of relatively slow risetime; the propagation delay appeared to be fixed with respect to the time at which the trigger pulse reached the bias level (in this case 0.56 volts) rather than some appreciably higher value.

The trigger pulse used had some overshoot, and the amplitude quoted in figure 8 is the maximum; over the first 5 nanoseconds the amplitude did not change by more than 10% of this maximum. As such, it is evident that the time jitter and threshold width, as well as the voltage at which the propagation delay begins to increase, must be considered as upper limits to the actual values.

The results were independent of the trigger length for values above 10 nanoseconds (the minimum obtainable with the pulse generator) which is not surprising since this exceeds the propagation time. It was noted, however, that pulses whose length was of the order of or less than the propagation delay did have the effect of lengthening that delay.

5.4 Conclusions

Clearly the avalanche circuit has very sharp discrimination characteristics, and exhibits at most small variations and jitter in the time of triggering near the bias level. For larger triggers, the jitter is certainly less than 0.5×10^{-10} seconds.

Of especial interest is the fact that it fires at a time directly related to the time at which the trigger pulse reached a certain (preset) voltage. By triggering at different points on the leading edge of the photomultiplier pulse, time resolution can be found as a function of this alone - that is at constant photomultiplier gain.

PART II: RECOVERY

5.5 Introduction

In section 3.4, it was noted that during an actual run the reference "spectrum" could be analysed to yield the counting-rate dependence of the system. Two properties are actually found: the dead time and the distortion time. The former is the length of time following a firing during which refiring is impossible; while the latter is a subsequent time during which refiring causes an untrue result.

5.6 Method of Analysis

At zero counting-rate in the photomultipliers, N reference coincidences appear in the reference spectrum and are primarily in, say, two kicksorter channels. At a known counting-rate, let N_δ be the number of reference coincidences which do not appear in the spectrum; and let N_ε be the number which appear outside the central channels. Then, if N_1 and N_2 are the counting-rates for each avalanche, elementary reasoning gives the following expressions for the dead time, t_δ, and the distortion time, t_ε:

$$t_\delta = \frac{N_\delta}{N(N_1 + N_2)}$$

$$t_\varepsilon = \frac{N_\varepsilon}{N(N_1 + N_2)}$$

where it is assumed that t_δ and t_ε are the same for both avalanches.

5.7 Results

Calculations at several different counting rates give the following approximate results: $t_\delta = 10$ µsec.

$t_\varepsilon = 30$ µsec.

This value for the dead time agrees exactly with the time to recharge capacitor C (see figure 1).

5.8 Discussion

Clearly, the circuit as it stands cannot be successfully used at very high counting rates. However, at the expense of certain other qualities, this is easily remedied:

Slight improvement may be obtained simply by decreasing the value of C and using a shorter clipping line; the consequences would, of course, include a decrease in the time range;

Consulting the references of section 2 will reveal a number of more extensive changes which could be made to decrease the recovery time. For most lifetime measurements, though, the present circuit is quite adequate.

PART III: LINEARITY

5.9 Limiter Pulse

The sum pulse at the output of the limiters, for reference coincidences, could be studied using the sampling oscilloscope. For maximum overlap (60 nanoseconds) the pulse was flat to within 5% over its entire length, and to within 2% over the central 45 nanoseconds.

5.10 Calibration

By varying the delay in the reference circuit, the height of the time analogue pulse (actually the kicksorter channel into which it falls) can be calibrated as a function of time delay. The relationship was linear to within one percent for a range of 45 nanoseconds.

FIGURE 8

above: The percentage of trigger pulses which fire the avalanche is plotted as a function of their amplitude.

below: Also plotted as a function of the trigger pulse amplitude is the relative propagation delay. The length of the vertical double lines corresponds to the jitter - being the full width at half maximum of the peak in the kicksorter time spectrum. See section 5.2 .

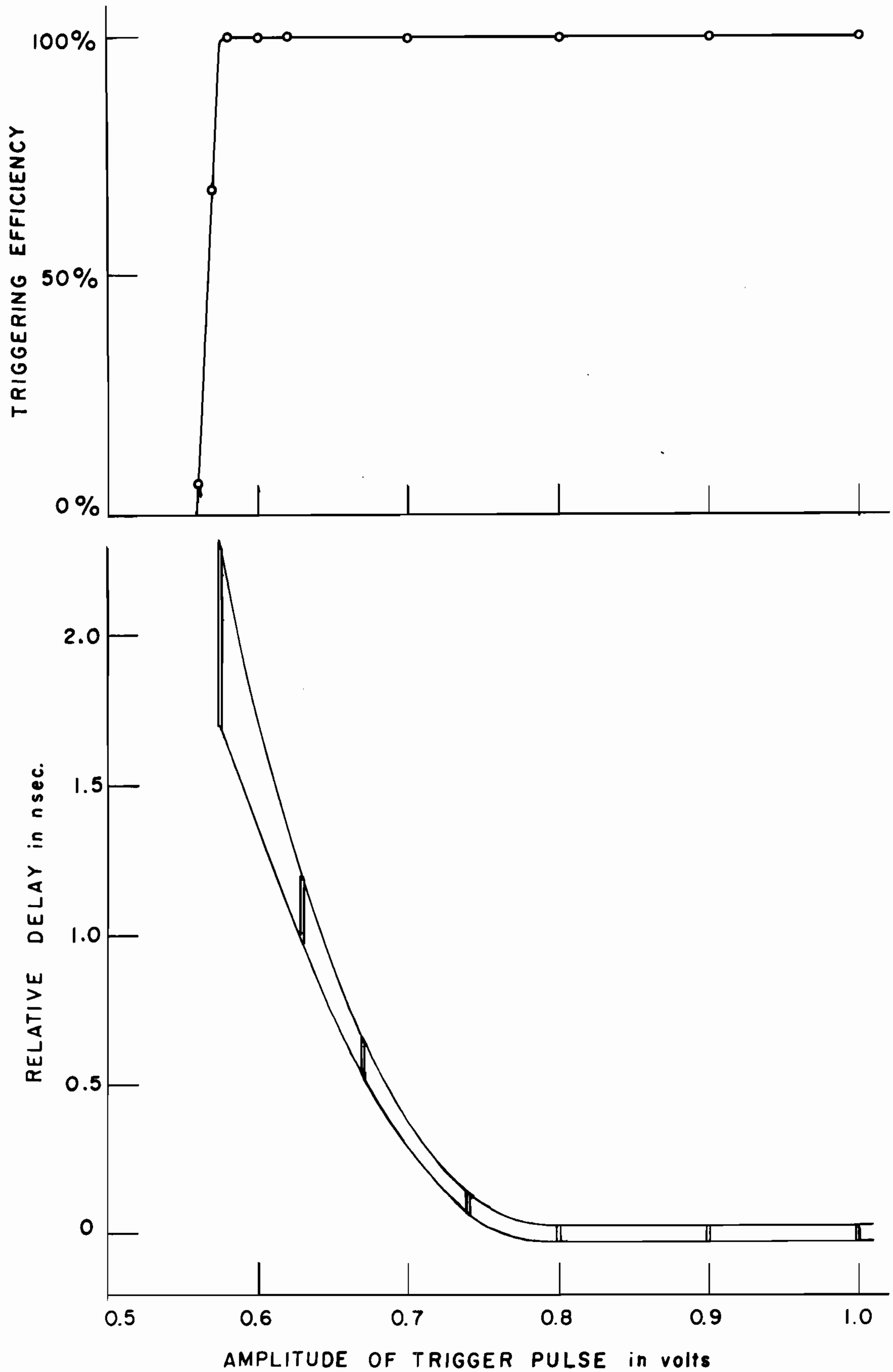

100%
50%
0%
TRIGGERING EFFICIENCY
2.0
1.5
1.0
0.5
0
RELATIVE DELAY in nsec.
0.5
0.6
0.7
0.8
0.9
1.0
AMPLITUDE OF TRIGGER PULSE in volts

FIGURE 8

6. TIME RESOLUTION OF THE SCINTILLATION COUNTERS

6.1 Introduction

Since the time jitter of the avalanche transistors and their associated circuitry has been established as being less than 0.5 x 10^{-10} seconds (see figure 8), the measured width (resolution) of a prompt coincidence curve will be almost entirely due to the properties of the scintillators and photomultipliers. It has also been established that the coincidence circuit is activated - that is, the avalanches are fired - at that time at which a certain definite charge is collected on the anode of the photomultiplier.

In their extensive theoretical analysis of time resolution, Gatti and Svelto (1959) have considered just such a method for activating the coincidence circuit (referred to as method B in their paper) and, by including photomultiplier and scintillator properties, they have worked out the dependence of resolution on the ratio of the "activation" charge to the average total charge collected on the anode for the desired pulse. It is noteworthy that this ratio is normally written as C/R, while R is defined as the average number of electrons emitted from the photocathode of the multiplier tube per scintillation; thus C must also be defined to be independent of the current amplification of the tube. In order to apply their results, the following properties are defined: τ is the decay time of the scintillator; λ is the width of the S.E.R. (single electron response) for the phototube; and ε_{ph} is the standard deviation of the time separation between the emission of one photoelectron and the arrival of the centroid of the S.E.R. at the anode.

Gatti and Svelto, and more recently Bartl and Weinzierl (1963), show several calculated curves of resolution as a function of C/R for particular chosen values of τ/ε_{ph} and λ/ε_{ph}. Depending on the choice, these show the optimum resolution being obtained for C/R between 0.05 and 0.3. Experimental investigations have been made by Schwarzschild (1961) and by Bartl and Weinzierl; both show the appropriate functional dependence on C/R. The former did not attempt numerical agreement, while the latter did not achieve good agreement using reasonable values for photomultiplier and scintillator properties.

6.2 Results

C.B.S. CL1055 photomultiplier tubes were used with 1" diameter x 1" NE102 plastic scintillators; the experimental arrangement was as shown in figure 5. The resolution of Co^{60} prompt curves which were recorded at different avalanche bias settings is plotted in figure 9. The theoretical curve shown in the same figure was arrived at as follows: The values $\tau = 3.5 \times 10^{-9}$ sec, $R = 350$, $\varepsilon_{ph} = 3 \times 10^{-10}$ sec were quoted by Bartl and Weinzierl for an identical scintillator with the Philips 56 AVP phototube; of the resultant calculated curves which they included, the best fit to the present results was for $\lambda = 0.9 \times 10^{-9}$ sec. This is quite reasonable and, considering the nature of the calculations, the agreement is good. It might also be noted that the decrease in the slope for larger values of C/R, which does not appear in the calculated curve, was observed by Schwarzschild as well.

FIGURE 9 :

The time resolution of the scintillation counters is plotted as a function of C/R - the ratio of the charge collected on the anode when the avalanches fire to the average total charge for a desired pulse. The conditions for the fitting of the theoretical curve are described in section 6.2.

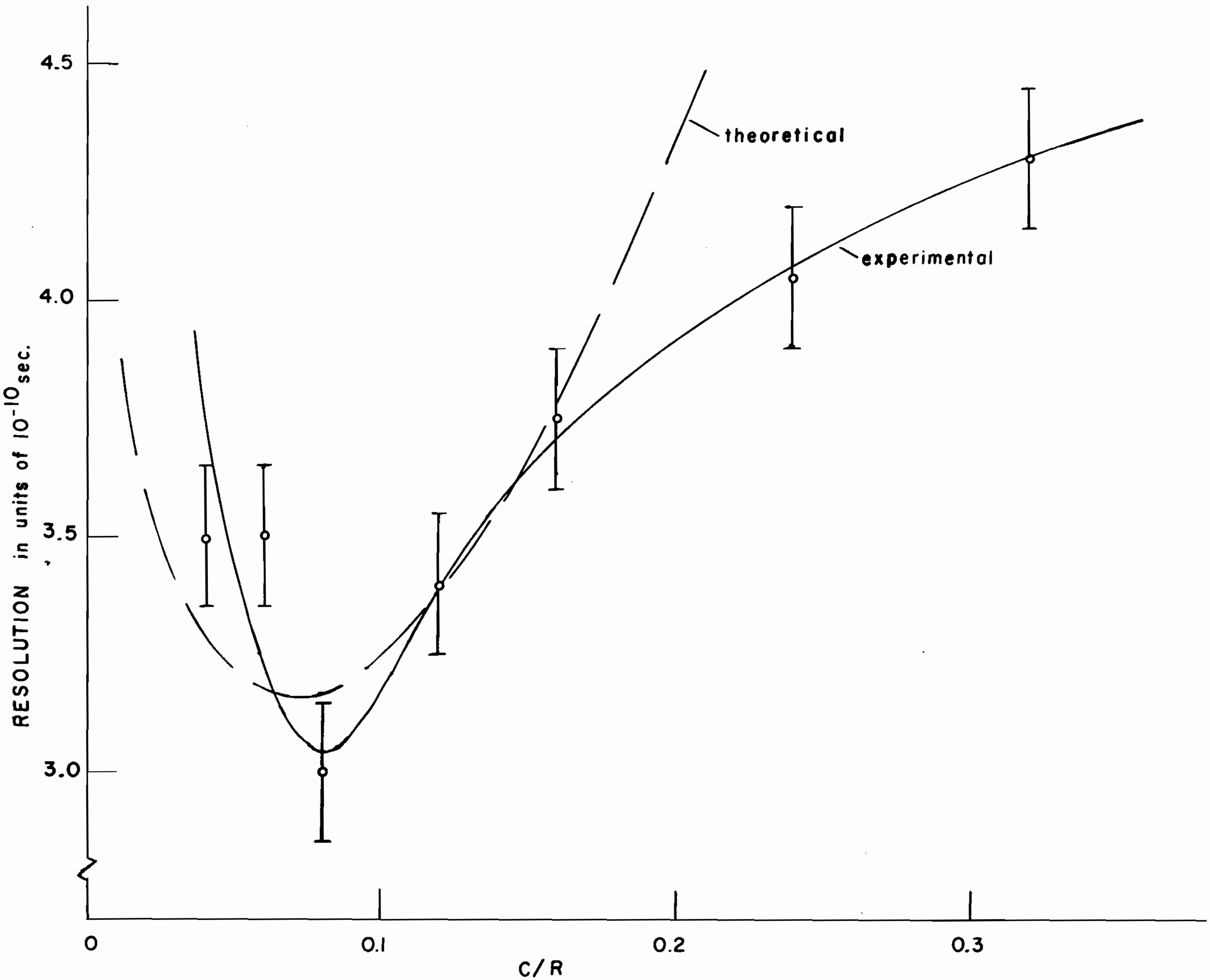

4.5
4.0
3.5
3.0
RESOLUTION in units of 10^{-10} sec.
theoretical
experimental
0
0.1
0.2
0.3
C/R

FIGURE 9

7. LIFETIME MEASUREMENT

7.1 Introduction

It has been shown by Bell and Jørgensen (1960) that the decay curve for the annihilation of positrons in aluminum is complex, exhibiting two lifetimes. Their results indicate that the mean life of the primary component is $1.9 \pm 0.2 \times 10^{-10}$ sec, while for the secondary component (intensity: 6.5%) it is approximately 3.9 $\times 10^{-10}$ sec. The former represents very nearly the lower limit which should be accurately measurable with the equipment and so provides a good test of it. On the other hand, an exact determination of the secondary component relies strongly on the counting-rate independence of the system: The effect of the distortion time will be to form a tail to the decay curve which could increase, or possibly completely create, a secondary lifetime. Bell and Jørgensen overcame this difficulty by using a pile-up detector which rejected all singles counts which came within a certain time of another count. For the present measurements no such method was used and, considering the relatively long distortion time, poorer results for the secondary component might be expected.

7.2 Procedure and Results

A drop of $Na^{22}Cl$ was deposited on a strip of Alcoa aluminum foil and evaporated to dryness; the foil was then folded to a thickness which prevented the escape of positrons. Coincidences were recorded between the 1.28 MeV γ's and the 511 KeV annihilation radiation.

The shape of the reference spectrum indicated that in the time region of interest, the tail (resulting from t_δ) could be closely approximated by an abnormally high, but constant, background. The results, after subtraction of this "background", are shown in figure 10. The full width at half maximum of the prompt curve is 5×10^{-10} sec and the right hand slope corresponds to a mean life of 1×10^{-10} sec. The mean lives are then read directly from the logarithmic slope of the delayed curve - the weaker component being fitted first to agree as nearly as possible with the points in the tail and to make the primary component linear over three decades. The resultant values for the mean lives are $2.0 \pm 0.2 \times 10^{-10}$ sec and $4.0 \pm 0.5 \times 10^{-10}$ sec (intensity: 10 ± 4 %).

7.3 Conclusions

These results agree with those quoted by Bell and Jørgensen, and the behaviour of the system was much as expected. The fact that the counting-rate dependence in this case could be so easily corrected for allowed a better measurement of the second lifetime than might have been expected, and this demonstrates the usefulness of recording the reference spectrum. The "background" was small enough (less than 0.4% of the maximum) that its subtraction had no effect on the primary lifetime, and so in those cases - by far the majority - where only a single lifetime is present, no correction is necessary.

FIGURE 10 :

The delayed coincidence curve is shown for the annihilation of positrons in aluminum. Also shown is a normalized prompt curve obtained for identical experimental conditions with Co^{60}. See section 7.2 .

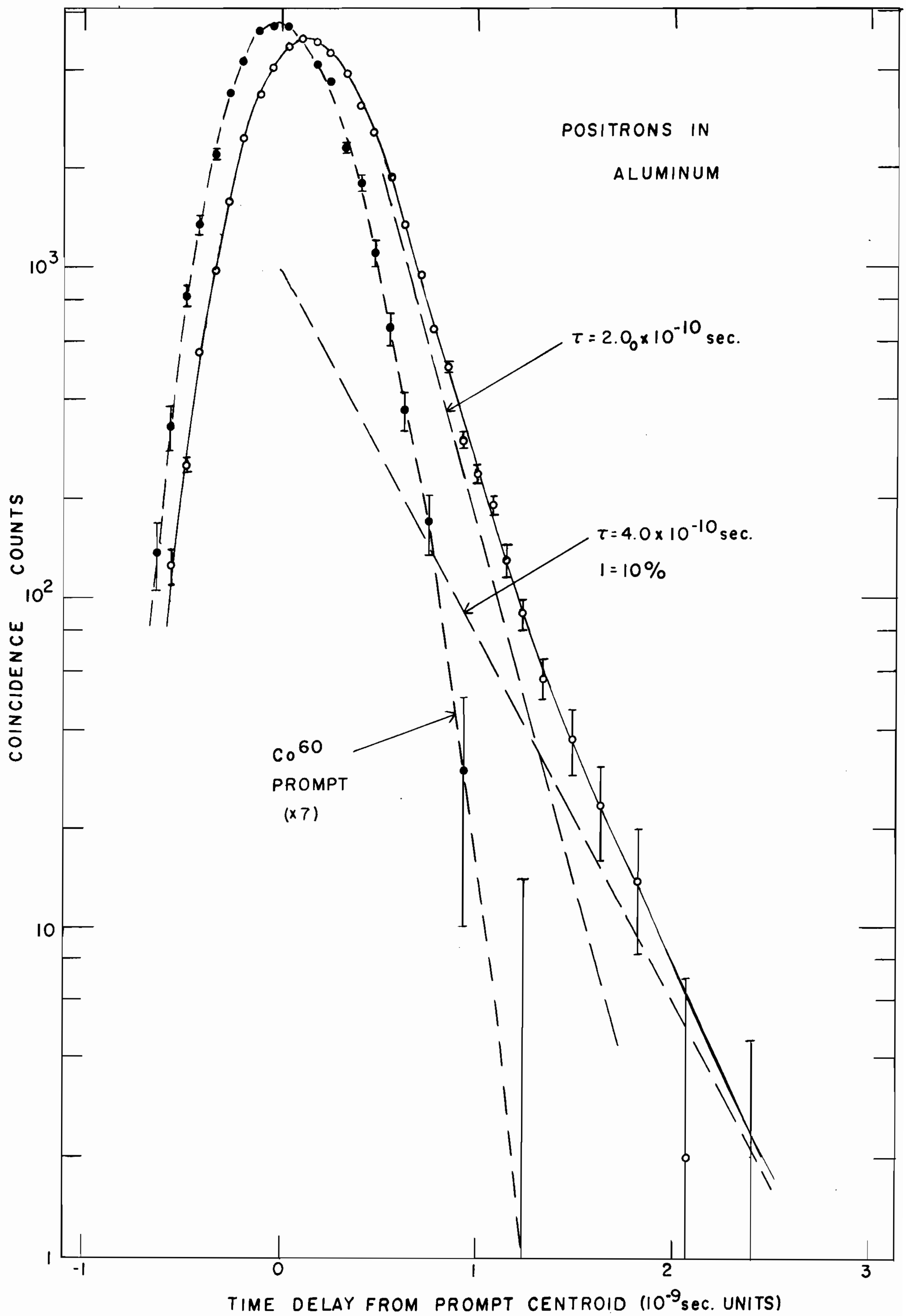

POSITRONS IN ALUMINUM
τ = 2.0₀ x 10⁻¹⁰ sec.
τ = 4.0 x 10⁻¹⁰ sec.
I = 10%
Co 60 PROMPT (x 7)
COINCIDENCE COUNTS
10³
10²
10
1
-1
0
1
2
3
TIME DELAY FROM PROMPT CENTROID (10⁻⁹ sec. UNITS)

FIGURE 10

8. SPECTROMETER TIME RESOLUTION

8.1 Procedure

In order to measure the time of flight corresponding to the various diaphragms of the spectrometer, an I^{131} source was used. I^{131} decays with an eight day half-life, by electron emission, to excited states of Xe^{131}. The most prominent (88%) β branch has an end point of 608 KeV and leaves Xenon in a 364 KeV state which decays principally (90%) to the ground state; the half-life is known to be 14 picoseconds (W.D. Hamilton, 1961). Coincidences were taken between the 364 KeV γ's and a part of the β continuum centred around 300 KeV; for the present purposes they may be considered prompt.

Prompt curves were recorded for those diaphragms with sufficient transmission, and their centroids compared to that of a prompt curve taken with all diaphragms closed and the lead shield (figure 7) removed. Since the path length in the latter case could be readily measured, and the energy of the electrons counted was known, the path lengths - or the time of flight - in the other cases could then be found.

8.2 Results

The transmission for each diaphragm was measured for the present experimental situation and the results are listed in Table II*. There is a discrepancy between the value for diaphragm 10 in this listing and the one in Table I, but this is probably caused by a slightly different positioning of the source. It should be noted that for these readings a baffle had been introduced between the pole pieces to

---

*Table II appears with figure 12.

prevent low energy electrons from making a double loop and focusing at the detector; this baffle also had the effect of stopping all electrons for diaphragm numbers below 6.

Strictly speaking, one can only directly relate centroid shift to path length if the transmission over each diaphragm opening is uniform. It was felt, however, that no correction was necessary in this case: The only diaphragm for which uneven transmission might have been a factor is number 6; yet the transmission of number 5, as given in Table I, is such as to suggest that the asymmetry of 6 is not too great. Certainly, any resultant error would be small compared to purely statistical errors.

The measured path lengths are shown in figure 11. In the same figure are shown calculated path lengths as a function of diaphragm number for several different pole-piece profiles; the relevant profiles are included (they are symmetric about their centre line). The method for calculating the path lengths is included in the following sub-section but it is evident from the figure that it is quite a sensitive function of the profile shape. It is equally evident that a good fit to the experimental points can be made only with the actual profile that was used. The conditions for the best fit will also appear in 8.3 .

The inherent time resolution for any diaphragm or combination of diaphragms is now defined as the full width of an (assumed) rectangular time distribution over that opening for electrons travelling at the velocity of light. The values for resolution derived from figure 11 are given in Table II; and a plot of resolution against transmission for all possible diaphragm combinations appears as figure 12.

8.3 Path Length Calculations

In order to calculate the path length of an electron moving from source to detector, a number of assumptions must be made about the magnetic field in the two regions through which it moves. Between the pole pieces the field is proportional to 1/r, where r is the perpendicular distance from the source-focus axis, and it is assumed that this 1/r dependence extends all the way to the edge of the profile. Beyond this edge, in the second region, the field drops off rapidly in some manner towards the axis. It is the assumption about the manner of this drop-off which most strongly affects the calculations.

a) "Ideal" Spectrometer: Let it be assumed that the field is zero everywhere beyond the pole pieces. Path length calculations proceed as follows: The trajectory is expressed parametrically in terms of θ, which is the angle between the axis and the direction of motion of the electron. The equations of motion in the 1/r field, which have been worked out by Kofoed-Hansen <u>et al</u> (1950), are then integrated to give the path length in that region,

$$S_i = 2\, z_f \frac{b\left[V(b,\pi-\theta_s) - V(b,0)\right]}{b\, U(b,\theta_s) - \cot\theta_s \exp(-b\cos\theta_s)} \quad ; \qquad (3 - A)$$

where the integrals,

$$U(b,\theta) = \int_{\pi}^{\theta} \cos\psi \exp(-b\cos\psi)\, d\psi$$

$$V(b,\theta) = \int_{\pi}^{\theta} \exp(+b\cos\psi)\, d\psi \, ,$$

appear frequently in calculations with this kind of spectrometer and have been tabulated by A.H. Jaffey et al (1960); and where

z_f is the distance of the source from the centre of the spectrometer,

θ_s is the value of θ at which the electron enters the $1/r$ field, and

b is a constant for the spectrometer (= 0.7).

Clearly, since θ is a constant outside the field, then θ_s is equal to the angle of emission from the source, and so S_i may be calculated as a function of this angle. Using the analytic expression for the profile shape (also derived by Kofoed-Hansen et al), the path length outside the field, S_o, may also be determined as a function of the angle of emission. $S = S_o + S_i$ is plotted against diaphragm number in figure 11. (The relationship between angle of emission and diaphragm number - for this approximation - has already been given in Table I.)

It is evident, however, that the assumption of an "ideal" spectrometer is not at all realistic; the difference between the actual profile shape and the calculated "ideal" one (see figure 11) is testimony to the assumption's invalidity.

b) Actual Spectrometer: In fact, the electrons will be acted upon by some field outside the pole pieces. Even if it were possible to express the exact fringing field, though, finding the resultant profile shape would be prohibitively difficult. Nevertheless, the actual profile shape is known - having been found empirically - and using it in place of the analytic expression used in (a), S may be found without the necessity for making any assumptions about the precise nature of the drop-off in the field beyond the pole pieces:

Suppose an electron leaves the source at an angle θ_o; it will have been turned through an additional angle θ_δ before reaching the profile edge, so that $\theta_s = \theta_o + \theta_\delta$. Kofoed-Hansen et al have estimated that θ_δ is of the order of the gap width (i.e. 20°). From the equations of motion in the 1/r field, a value for θ_s may be found for every point on the profile edge, and the corresponding S_i calculated from (3 - A) (using for z_f the distance from the centre of the spectrometer at which the tangent to the trajectory at that point cuts the axis - i.e. the apparent source position). Since θ_δ will be quite small, S_o is given very closely by twice the linear distance from the point on the profile to the actual source position, subtracting a correction for the finite size of the detector. Thus S is found as a function of θ_s.

By making simple approximations to the fringing field, it can be shown that θ_δ is practically independent of θ_o. Consequently, by sliding the horizontal axis of the plot of calculated $S(\theta_s)$ along that axis of the experimental plot, a fit should be obtained. The best fit is shown in figure 11. However, the so-called angle of emission previously associated with each diaphragm (θ in figure 7 and table I) will not now correspond to the actual θ_o, since some bending of the trajectory has taken place before the diaphragm is reached. If $\Delta = \theta_s - \theta$ for the best fit, then one would expect Δ to be somewhat less than θ_δ. This turns out to be quite consistent with the value $\Delta = 14°$ found in this case.

c) "Flat" Spectrometer: To test the sensitivity of these calculations to the profile shape, they were also performed for a flat profile (also shown in figure 11); the best fit was very poor and led to a value of $\Delta = 2°$.

FIGURE 11 :

On the same graph as the experimentally measured points is shown the calculated path length (solid curve) using the actual profile shape and the method described in section 8.3. The dashed curves are similarly calculated for other profiles. Δ is the angle through which the electron trajectory is turned between diaphragm and profile edge - its value for the best fit is shown.

Outlines of the profiles involved are shown below the graph - only half of each being shown since they are symmetric about their centre line.

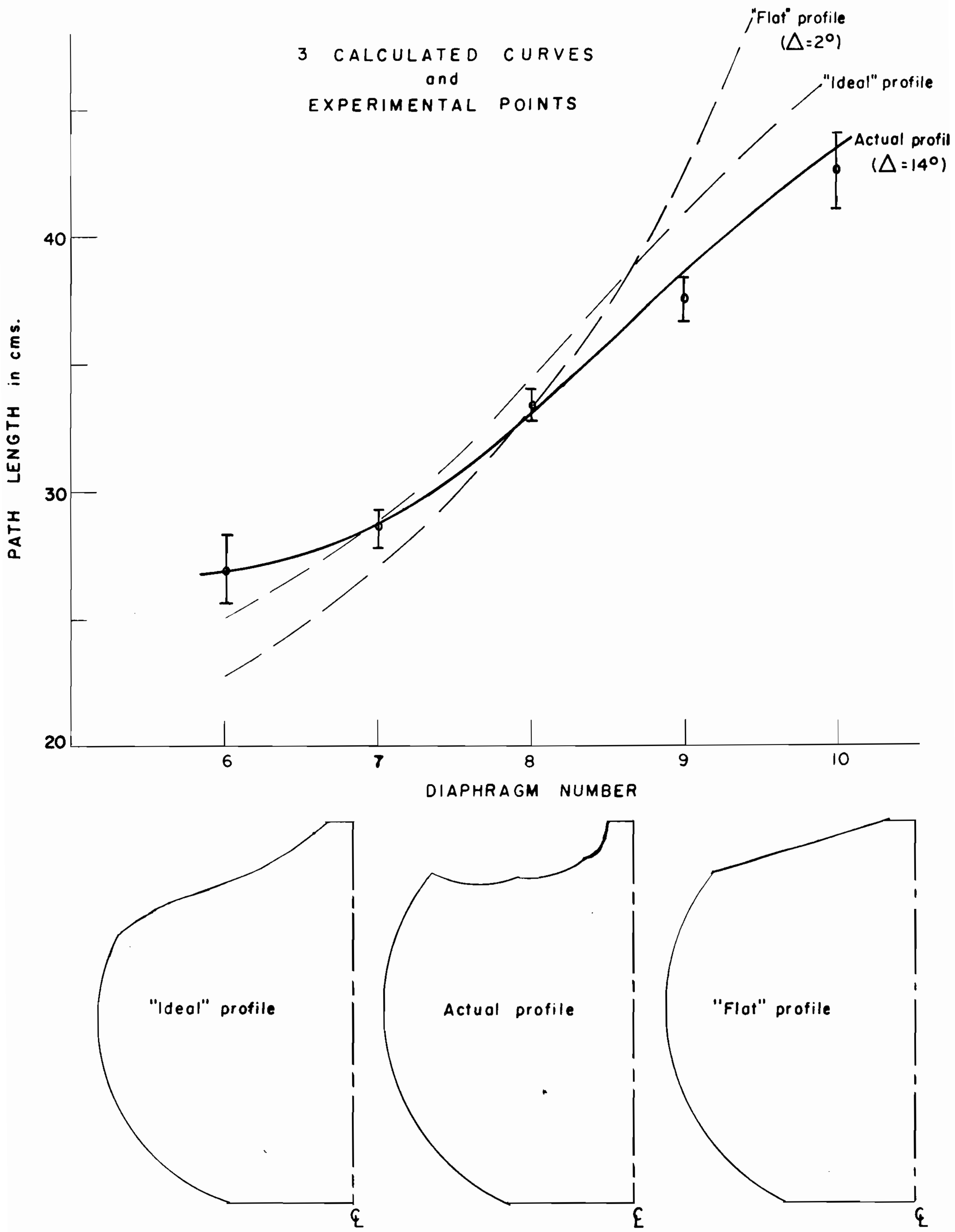

3 CALCULATED CURVES
and
EXPERIMENTAL POINTS
"Flat" profile
(Δ=2°)
"Ideal" profile
Actual profil
(Δ=14°)
PATH LENGTH in cms.
40
30
20
6
7
8
9
10
DIAPHRAGM NUMBER
"Ideal" profile
Actual profile
"Flat" profile

FIGURE 11

<u>TABLE II</u> :

The inherent time resolution - defined in section 8.2 - and % transmission for each significant diaphragm of the spectrometer are listed.

<u>FIGURE 12</u> :

Using the values in Table II, the time resolution is plotted as a function of transmission. The numbers beside the points refer to the diaphragms which must be utilized. See section 8.2 .

TABLE II

TIME RESOLUTION and TRANSMISSION
for the ORANGE SPECTROMETER

Diaphragm No.	Inherent Resolution ($\times 10^{+10}$ sec.)	Transmission (%)
6	0.2	.08
7	1.0	.16
8	1.8	.22
9	1.7	.19
10	1.4	.19
		(all values ± .02)

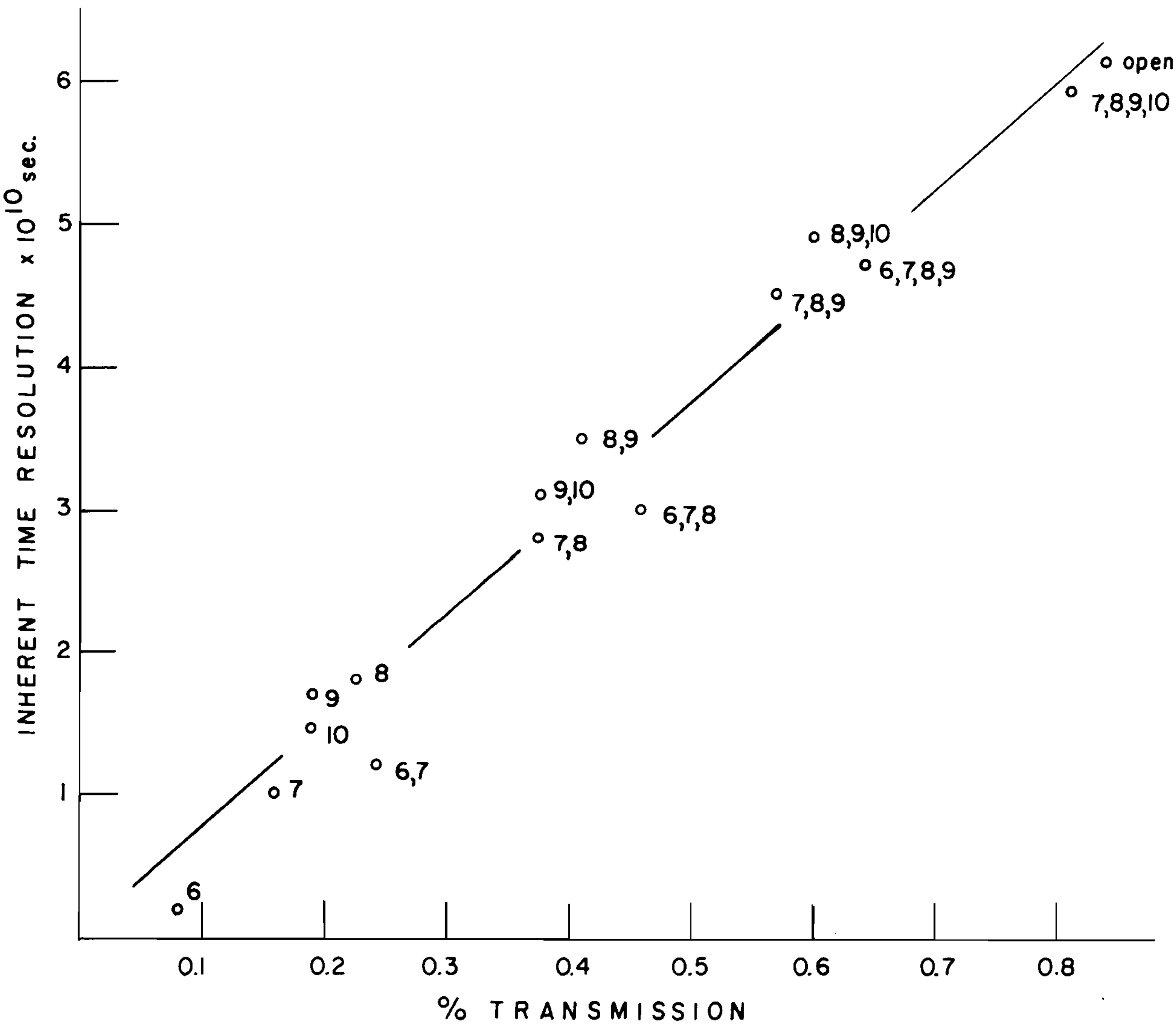

FIGURE 12

9. OVERALL TIME RESOLUTION

The time distribution of electrons at the focus of the spectrometer will be approximately rectangular. In section 8.2, the inherent time resolution of the instrument was defined for electrons travelling at the velocity of light; similarly the resolution, R_s, at any electron energy will be taken as the full width of the distribution at that energy. Clearly R_s is proportional to $1/\beta$ where βc equals the electron velocity.

Now, if a coincidence circuit with a resolution R_c is used in conjunction with the spectrometer, calculations by P. Onno (1962) show that the resolution of the combination will be given by

$$R = R_c + 0.23\,(R_s/R_c)\,R_s\ .$$

In section 6 the resolution of the scintillator, photomultiplier, and avalanche coincidence circuit has been discussed; the values quoted were for coincidences between γ-rays of slightly more than 1 MeV (to be exact: 1.17 and 1.33 MeV). It is well known that such resolution becomes worse as the amount of energy lost in the scintillator decreases. If E is the energy lost in the phosphor, Gatti and Svelto (1959) state that the width of a prompt curve should be proportional to $1/(E)^{1/2}$; Schwarzschild (1961) found experimentally that the variation was not so great as that. Considering the resolution, R_c, purely as a function of the electron energy (i.e. at a fixed energy loss in the γ detector), Schwarzschild's results indicate that, down to 300 KeV, R_c increases no slower than $1/\beta$; at lower energies, though, its rate of increase is slower.

Evidently, in most cases the major contribution to the total resolution, R, will be from R_c and not R_s. It is only when measuring coincidences between high energy γ's and electrons with an energy considerably less than 300 KeV that R_s may dominate.

Prompt curves were recorded for I^{131} (300 KeV β^-; 364 KeV γ) and for Na^{22} (300 KeV β^+; 1.28 MeV γ) using diaphragm 8; the widths were 7×10^{-10} and 4×10^{-10} seconds respectively. The spectrometer contribution to these values was 3% and 8% of the total. For higher transmission (see figure 12), the contribution does increase but in general will remain small.

REFERENCES

BARTL, W. and WEINZIERL, P. 1963. Rev. Sci. Instr. 34, 3.

BELL, R.E., GRAHAM, R.L., and PETCH, H.E. 1952. Can. J. Phys. 30, 35.

BELL, R.E. and JØRGENSEN, M.H. 1960. Can. J. Phys. 38, 652.

BRAMSON, M. 1962. Proc. I.R.E. NS-9, 35.

DEMILLE, G.R. Details of the construction and properties of the Orange Spectrometer will appear shortly in the form of a Ph. D. Thesis, McGill University.

EL-WAHAB, M.A. and KANE, J.V. 1962. Nuclear Instr. 15, 15.

FULLWOOD, R. 1960 Rev. Sci. Instr. 31, 1186.

GATTI, E. and SVELTO, V. 1959. Nuclear Instr. 4, 189.

GRAHAM, R.L., GEIGER, J.S., BELL, R.E., and BARTON, R. 1962. Nuclear Instr. 15, 40.

HAMILTON, W.D. 1961. Proc. of Phys. Soc. 77, 610.

HENEBRY, W.M. 1961. Rev. Sci. Instr. 32, 1198.

HILBORN, J. 1954. Ph. D. Thesis, McGill University (unpublished).

JAFFEY, A.H., MALLMANN, C.A., SUAREZ-ETCHIPARE, J., and SUTER, T. 1960. Argonne National Laboratory ANL - 6222.

KOFOED-HANSEN, O., LINDHARD, J., and NIELSEN, O.B. 1950. Dan. Mat. Fys. Medd. 25, no. 16.

MILLER, H.W. and KERNS, Q.A. 1962. Rev. Sci. Instr. 33, 877.

MILLER, S.L. and EBERS, J.J. 1955. Bell System Tech. J. 34, 883.

NIELSEN, O.B. and KOFOED-HANSEN, O. 1955. Dan. Mat. Fys. Medd. 29, no. 6.

ONNO, P. 1962. M. Sc. Thesis, McGill University (unpublished).

REFERENCES (concluded)

SCHWARZSCHILD, A. 1961. Brookhaven National Laboratory BNL - 5715.

WEAVER, R.S. 1962. Ph. D. Thesis, McGill University (unpublished).